Intrinsic electrical, magnetic, and thermal properties of single-crystalline $Al_{64}Cu_{23}Fe_{13}$ icosahedral quasicrystal: Experiment and modeling

J. Dolinšek,[1] S. Vrtnik,[1] M. Klanjšek,[1] Z. Jagličić,[2] A. Smontara,[3] I. Smiljanić,[3] A. Bilušić,[3] Y. Yokoyama,[4] A. Inoue,[4] and C. V. Landauro[5]

[1]*J. Stefan Institute, University of Ljubljana, Jamova 39, SI-1000 Ljubljana, Slovenia*

[2]*Institute of Mathematics, Physics and Mechanics, Jadranska 19, SI-1000 Ljubljana, Slovenia*

[3]*Institute of Physics, Bijenička 46, P.O. Box 304, HR-10001 Zagreb, Croatia*

[4]*Advanced Research Center of Metallic Glasses, Institute for Materials Research, Tohoku University, Katahira, Aobaku, Sendai 980-8577, Japan*

[5]*Faculty of Physical Sciences, National University of San Marcos, P.O. Box 14-0149, Lima 14, Peru*

(Received 18 April 2007; published 3 August 2007)

In order to test for the true intrinsic properties of icosahedral *i*-Al-Cu-Fe quasicrystals, we performed investigations of magnetism, electrical resistivity, thermoelectric power, and thermal conductivity on a single-crystalline $Al_{64}Cu_{23}Fe_{13}$ quasicrystal grown by the Czochralski technique. This sample shows superior quasicrystallinity, an almost phason-free structure, and excellent thermal stability. Magnetic measurements revealed that the sample is best classified as a weak paramagnet. Electrical resistivity exhibits a negative temperature coefficient with $\rho_{4\ K}=3950\ \mu\Omega$ cm and $R=\rho_{4\ K}/\rho_{300\ K}=1.8$, whereas the thermopower exhibits a sign reversal at $T=278$ K. Simultaneous analysis of the resistivity and thermopower using spectral-conductivity model showed that the Fermi energy is located at the minimum of the pseudogap in the spectral conductivity $\sigma(\varepsilon)$. Thermal conductivity is anomalously low for an alloy of metallic elements. Comparing the physical properties of the investigated single-crystalline $Al_{64}Cu_{23}Fe_{13}$ quasicrystal to literature reports on polycrystalline *i*-Al-Cu-Fe material, we conclude that there are no systematic differences between the high-quality single-crystalline and polycrystalline *i*-Al-Cu-Fe quasicrystals, except for the hindering of long-range transport by grain boundaries in the polycrystalline material. The so far reported physical properties of *i*-Al-Cu-Fe appear to be intrinsic to this family of icosahedral quasicrystals, regardless of the form of the material.

DOI: 10.1103/PhysRevB.76.054201 PACS number(s): 61.44.Br, 71.23.Ft

I. INTRODUCTION

Although a stable icosahedral *i*-Al-Cu-Fe quasicrystal (QC) was discovered already in 1987,[1] preparation of a single *i*-Al-Cu-Fe QC from the melt had not been reported until 2000.[2,3] Growing QCs directly from the melt yields large centimeter-sized single grains of superior structural quality, containing neither high density of defects nor phason strain that are present in samples produced by rapid solidification techniques. While rapid solidification yields the material in a polycrystalline form (in *i*-Al-Cu-Fe, a typical grain size[4] is 60–100 μm), single grains of *i*-Al-Cu-Fe up to millimeter size were successfully prepared also by long-term annealing of the polycrystalline material.[5–7] The so-prepared single grains were reported to contain phason strain and porosity,[8] so that growing directly from the melt is preferable to prepare unstrained single-grain QCs. High-quality samples are of essential importance in revealing the intrinsic properties of QCs.

Due to its excellent thermal stability, *i*-Al-Cu-Fe is currently one of the best-studied icosahedral QCs. Most studies reported so far were performed on polycrystalline samples. The vast literature on the physical properties of *i*-Al-Cu-Fe includes investigations of the electrical resistivity and magnetoresistance,[4,7,9–15] thermoelectric power,[15–18] thermal conductivity,[4,15,19] magnetism,[9,14,20] and Hall coefficient.[7,11,15,16] Though polycrystalline samples may acquire quite high structural perfection through a proper thermal annealing procedure, rapid quenching to room temperature (RT) after annealing inevitably results in a strained material that also contains a too high thermal vacancy concentration for the RT conditions (i.e., the quenched-in vacancy concentration is in equilibrium for the much higher temperature of annealing). In addition, grain boundaries may hinder propagation of electrons and phonons, thus affecting long-range electrical and heat transport phenomena. In order to test for the true intrinsic properties of the *i*-Al-Cu-Fe QCs, it is desirable to compare the physical properties of the polycrystalline material to those measured on high-quality single-crystalline samples, where structural imperfections are largely absent. In this paper, we perform such a study by investigating magnetism, electrical resistivity, thermoelectric power, and thermal conductivity of a single-crystalline $Al_{64}Cu_{23}Fe_{13}$ icosahedral QC grown directly from the melt by the Czochralski technique. Based on x-ray and high-resolution transmission electron microscopy (HRTEM) structural evaluations,[21] this sample shows superior quasicrystallinity and an almost phason-free icosahedral structure.

II. SAMPLE SELECTION

Preparation of large single-crystalline icosahedral QCs with composition $Al_{64}Cu_{23}Fe_{13}$ by the Czochralski technique and annealing removal of strains has been described in detail in previous publications.[2,3] This composition was chosen because of its superior thermal stability (any secondary-phase precipitates in the as-grown material disappeared upon annealing[2]), so that it is considered to represent the ideal

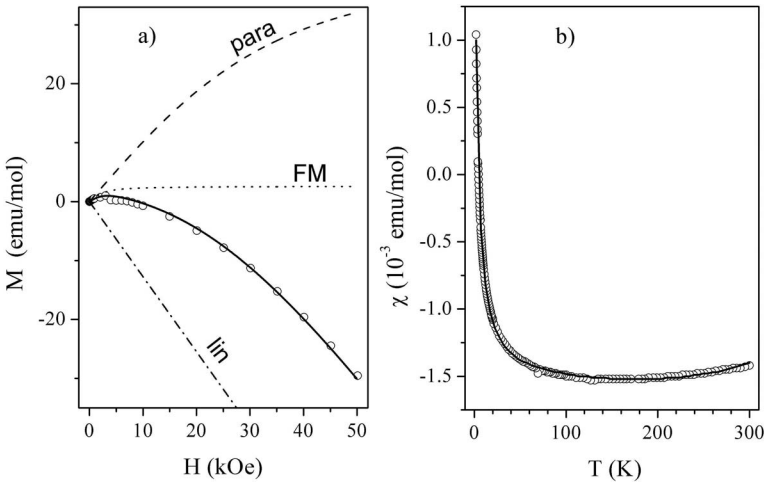

FIG. 1. (a) Magnetization M as a function of the magnetic field at $T=5$ K. The fit (solid line) was made with Eq. (1). The paramagnetic (para), ferromagnetic (FM), and linear (lin) contributions are shown separately. (b) Temperature-dependent magnetic susceptibility $\chi=M/H$ in a field $H=10$ kOe. The solid line is the fit with Eq. (2). The fit parameters are collected in Table I.

icosahedral composition. The crystal was pulled out of the molten alloy of composition $Al_{57.7}Cu_{37.7}Fe_{3.5}Si_{1.1}$ [where Si was added to restrain crystallization of $(Al+Cu)_{13}Fe_4$] with the speed of 0.05 μm/s at 1073 K and the growth direction was parallel to the threefold symmetry axis. The investigated crystal of 2 mm diameter and 10 mm length showed a faceted cylindrical shape and its quasicrystallinity was evaluated by x-ray diffraction analysis.[21] The full widths at half maximum (FWHMs) of the Bragg reflections along the two-, three-, and fivefold symmetry directions exhibited no $Q_\parallel$ and $Q_\perp$ dependence, where $Q_\parallel$ is the real scattering vector and $Q_\perp$ is the phason momentum. Furthermore, peak shifts from ideal Bragg positions were not detected. This showed that neither random- nor linear phason strain is present in the structure. The phason-free structure on the atomic scale was confirmed by HRTEM imaging,[21] which showed highly ordered patterns with no kinks or dead ends in the atomic rows on the selected scale of 17×23 nm^2. Therefore, the investigated single-crystalline $Al_{64}Cu_{23}Fe_{13}$ icosahedral QC has an almost phason-free quasicrystalline structure and shows superior quasicrystallinity on both macro- and microscopic scales.

III. MAGNETISM

Magnetic properties of single-crystalline $Al_{64}Cu_{23}Fe_{13}$ were studied by performing measurements of the magnetization as a function of magnetic field, $M(H)$, and the magnetic susceptibility as a function of temperature, $\chi(T)$, using a superconducting quantum interference device 5 T magnetometer. The $M(H)$ curve at $T=5$ K with the magnetic field parallel to the threefold symmetry direction is displayed in Fig. 1(a). At magnetic fields not too close to zero, the $M(H)$ behavior is predominantly diamagnetic (exhibiting negative slope), whereas at low fields, a positive curvature with a maximum at $H=3$ kOe is observed. This indicates the presence of a small fraction of localized paramagnetic moments in the sample. An attempt to reproduce the $M(H)$ curve with the sum of a diamagnetic linear term and a Curie paramagnetic term failed in the low-field regime (below 10 kOe), because the magnetization growth was much too fast to be described by a Brillouin function assuming either Fe^{2+} or Fe^{3+} localized moments. It was obvious that the $M(H)$ curve contains also a small ferromagnetic (FM) component. This component originates from a thin FM oxide layer, which quite commonly forms at the surfaces of Fe-containing alloys exposed to ambient atmosphere. The $M(H)$ dependence of the FM component can still be modeled by a Brillouin function but with an unphysically large angular momentum J. The FM saturation magnetization is, however, well defined and can be used to estimate the amount of FM moments in the total magnetization. The fit [solid line in Fig. 1(a)] was performed with the expression

$$M = M_1 B(g_1, J_1) + M_2 B(g_2, J_2) + kH. \quad (1)$$

Here, $B(g_1,J_1)$ is the Brillouin function describing the Curie magnetization of a set of localized paramagnetic moments of angular momentum J_1 and Landé g factor g_1, whereas M_1 is their saturation magnetization. $B(g_2,J_2)$ and M_2 are the corresponding quantities for the FM component, whereas k is the magnetic susceptibility associated with terms linear in the magnetic field. Generally, $k=\chi_{dia}+\chi_c$ contains a negative Larmor diamagnetic term χ_{dia} due to atomic cores and a contribution due to spin and orbital magnetism of conduction electrons χ_c. In the fit procedure, the paramagnetic moments were assumed to be Fe^{2+} and the corresponding values $J_1=2$ and $g_1=2$ were taken as fixed, whereas the fit-determined Curie saturation magnetization amounted to $M_1=40.6$ emu/mol. For the FM component, $g_2=2$ was taken as fixed, whereas the fit yielded $J_2=31$ (an unphysical value) and the FM saturation magnetization $M_2=2.9$ emu/mol. The linear term was determined as $k=-1.3\times10^{-3}$ emu/mol. The fit parameters are collected in Table I and the three contributions to the total $M(H)$ fit are displayed separately in Fig. 1(a). The fraction f of the paramagnetic Fe^{2+} moments in the sample can be estimated by comparing the M_1 value to the saturation magnetization for the case that all Fe atoms in the sample would carry full Fe^{2+} magnetic moments, wherefrom we obtain $f=1.4\times10^{-4}$. The FM fraction is smaller by a factor $M_2/M_1=1/14$, yielding $f_{FM}=1\times10^{-5}$. The smallness of this value supports the consideration that the FM component is due to a thin surface oxide layer. The Larmor diamagnetic contribution was estimated from literature tables[22] to

TABLE I. Parameters of the $M(H)$ and $\chi(T)$ fits from Figs. 1(a) and 1(b) using Eqs. (1) and (2).

$M(H)$						
M_1 (emu/mol)	J_1	g_1	M_2 (emu/mol)	J_2	g_2	k (emu/mol)
40.6	2	2	2.9	31	2	-1.3×10^{-3}
$\chi(T)$						
χ_0 (emu/mol)	C (emu K/mol)		θ (K)	A_1 (emu K^2/mol)		A_2 (emu K^4/mol)
-1.6×10^{-3}	1.1×10^{-2}		−2.3	-6.1×10^{-10}		2.5×10^{-14}

amount to $\chi_{dia}=-6\times10^{-4}$ emu/mol, which is a factor about 2 smaller than the fit-determined k value. The difference $k-\chi_{dia}=\chi_c=-7\times10^{-4}$ emu/mol is the estimated susceptibility of conduction electrons.

Magnetic susceptibility χ was investigated in the temperature interval between 300 and 2 K [Fig. 1(b)] in a magnetic field $H=10$ kOe. χ is negative (diamagnetic) in most of the investigated temperature range except below 7 K, where the Curie tail brings it to a positive value. The $\chi(T)$ data were analyzed by the expression

$$\chi = \chi_0 + \frac{C}{T-\theta} + A_1T^2 + A_2T^4, \tag{2}$$

where $C/(T-\theta)$ is the Curie-Weiss term due to the localized paramagnetic moments, with C being the Curie constant and θ the Curie-Weiss temperature. The terms A_1T^2 and A_2T^4 are the two lowest-order temperature corrections to the spin susceptibility of conduction electrons emerging from the temperature dependence of the chemical potential μ and the variation of the electronic density of states (DOS) with energy in the vicinity of the Fermi energy ε_F. Explicit forms of A_1 and A_2 can be found, e.g., in Ref. 23. The constant χ_0 contains the temperature-independent part of the conduction-electron susceptibility, the diamagnetic core susceptibility, and the FM contribution, which is already saturated in the applied field. The fit with Eq. (2) is excellent and is shown in Fig. 1(b), whereas the fit parameter values are collected in Table I. The small negative θ value should be considered as an additional fit parameter only, which slightly improves the fit. No other experimental results suggest any antiferromagnetic interaction between the magnetic moments.

The Curie constant C allows for an independent estimate of the fraction of magnetic Fe atoms in the sample. Assuming Fe^{2+} with the effective Bohr magneton number $p_{eff}=5.4$, we recalculate C (given in Table I in units of per mole of sample) in units of per mole of Fe (i.e., divide by 13, the number of Fe in one $Al_{64}Cu_{23}Fe_{13}$ unit). From the obtained value, we calculate the mean effective Bohr magneton number $\bar{p}_{eff}$ (the mean p_{eff} of all the Fe atoms in the sample) by using the formula[24] $\bar{p}_{eff}=2.83\sqrt{C}$. The magnetic Fe fraction is then obtained from $f=(\bar{p}_{eff}/p_{eff})^2=2.3\times10^{-4}$. This value is in reasonable agreement with the value obtained from the saturation magnetization ($f=1.4\times10^{-4}$), showing the precision of the analysis. The "residual" magnetic Fe fraction of the order 10^{-4} is still substantial, so that the investigated $Al_{64}Cu_{23}Fe_{13}$ sample should be classified as a weak paramagnet rather than a diamagnet. A practically identical magnetic Fe fraction ($f=2\times10^{-4}$) was reported also for polycrystalline $Al_{63}Cu_{25}Fe_{12}$ QC.[14]

IV. ELECTRICAL RESISTIVITY AND THERMOELECTRIC POWER

Electrical resistivity and thermopower of $Al_{64}Cu_{23}Fe_{13}$ were measured in a temperature interval between 315 and 4 K along the threefold symmetry direction and are displayed in Fig. 2. The resistivity [Fig. 2(a)] exhibits a negative temperature coefficient with a RT value $\rho_{300\ K}=2200\ \mu\Omega$ cm and $\rho_{4\ K}=3950\ \mu\Omega$ cm, so that the total increase is by a factor $R=\rho_{4\ K}/\rho_{300\ K}=1.8$. At 20 K, $\rho(T)$ exhibits a weakly pronounced maximum with the peak value $\rho_{20\ K}=4040\ \mu\Omega$ cm. The thermopower [the Seebeck coefficient $S(T)$] is displayed in Fig. 2(b) and exhibits an interesting feature of a sign reversal. Below 120 K, $S(T)$ is negative with a negative slope, whereas at 120 K, it exhibits a minimum and the slope is reversed. $S(T)$ consequently changes sign to positive at $T=278$ K.

For the theoretical analysis of $\rho(T)$ and $S(T)$, we shall use the spectral resistivity model of Landauro and Solbrig,[17,18,25] where both quantities are analyzed simultaneously by presuming a specific structure- and composition-related form of the energy-dependent spectral resistivity function $\rho(\varepsilon)$ [or its inverse, the spectral conductivity $\sigma(\varepsilon)=1/\rho(\varepsilon)$]. Using the Kubo-Greenwood formalism, the temperature-dependent electrical conductivity is calculated according to

$$\sigma(T) = \int d\varepsilon\sigma(\varepsilon)\left[-\frac{\partial f(\varepsilon,T)}{\partial\varepsilon}\right], \tag{3}$$

whereas the thermopower is obtained from

$$S(T) = -\frac{k_B}{|e|\sigma(T)}\int d\varepsilon\sigma(\varepsilon)\left[\frac{\varepsilon-\mu(T)}{k_BT}\right]\left[-\frac{\partial f(\varepsilon,T)}{\partial\varepsilon}\right]. \tag{4}$$

Here, $f(\varepsilon,T)=\{\exp[(\varepsilon-\mu)/k_BT]+1\}^{-1}$ is the Fermi-Dirac function and $\mu(T)$ is the chemical potential, which is written in the low-temperature representation as[26]

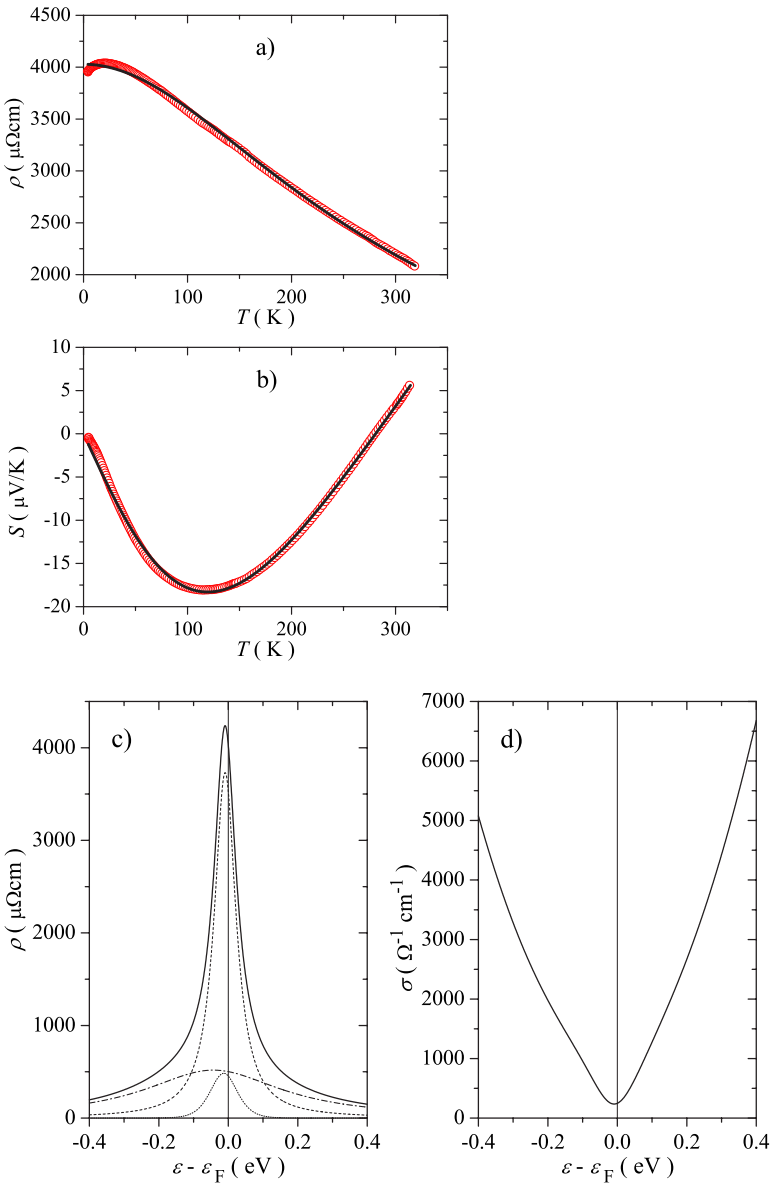

FIG. 2. (Color online) (a) Temperature-dependent electrical resistivity and (b) thermopower of the single-crystalline $Al_{64}Cu_{23}Fe_{13}$. The fits (solid lines) of both quantities were made simultaneously by the Kubo-Greenwood formalism using the spectral resistivity function $\rho(\varepsilon)$ displayed in (c). $\rho(\varepsilon)$ (solid line) is a superposition of two Lorentzians, shown by the dashed and dash-dot lines. The dotted bell-shaped curve at the bottom of the graph shows the thermal observation window $-\partial f/\partial\varepsilon$ (the derivative of the Fermi-Dirac function) at $T=300$ K. In (d), the spectral conductivity $\sigma(\varepsilon)=1/\rho(\varepsilon)$ is shown.

$$\mu(T) \approx \varepsilon_F - (k_B T)^2 \frac{\pi^2}{6}\left[\frac{d\ln n(\varepsilon)}{d\varepsilon}\right]_{\varepsilon_F} = \varepsilon_F - \xi T^2. \quad (5)$$

The electronic DOS $n(\varepsilon)$ is related to the spectral conductivity via the Einstein relation $\sigma(\varepsilon)=(e^2/V)n(\varepsilon)D(\varepsilon)$, with $D(\varepsilon)$ being the electronic spectral diffusivity. The only material-dependent quantity in Eqs. (3) and (4) is $\sigma(\varepsilon)$, so that a proper model of the spectral conductivity should reproduce both $\sigma(T)$ and $S(T)$ at the same time.

The shape of the spectral resistivity $\rho(\varepsilon)$ pertinent to *i*-Al-Cu-Fe was derived on the basis of *ab initio* calculations performed on the Cockayne model for the 1/1 approximant of the icosahedral Al-Cu-Fe phase.[17,18,25] In the vicinity of the self-consistently calculated Fermi energy ε_F, $\rho(\varepsilon)$ of the approximant exhibits two resistivity peaks: a broad one of width ~1 eV due to the Hume-Rothery stabilization mechanism and a narrow one of width ~100 meV due to chemical order of the subsystem of Fe atoms. The *ab initio* derived spectral resistivity could be modeled by a superposition of two Lorentzians,

$$\rho(\varepsilon) = A\left\{\left[\frac{1}{\pi}\frac{\gamma_1}{(\varepsilon-\delta_1)^2+\gamma_1^2}\right] + \alpha\left[\frac{1}{\pi}\frac{\gamma_2}{(\varepsilon-\delta_2)^2+\gamma_2^2}\right]\right\}, \quad (6)$$

where $1/\pi\gamma_i$ is the height of a Lorentzian, $2\gamma_i$ its FWHM, δ_i its position with respect to the Fermi energy (taken to be at the origin of the energy scale; $\varepsilon_F=0$), and α the relative weight of the Lorentzians. This shape of $\rho(\varepsilon)$, suitably scaled, was applied also to *i*-Al-Cu-Fe QCs.[17,18,25] The position of the narrow resistivity peak with respect to the Fermi energy is responsible for the anomalous electronic transport properties. As this peak is due to a specific distribution of Fe atoms in the structure, quasiperiodicity alone cannot account for the anomalous transport properties of *i*-Al-Cu-Fe QCs; a right chemical decoration is also needed. Fermi energy can be shifted on the scale of a few hundred meV by deviations

TABLE II. Parameters of the spectral resistivity $\rho(\varepsilon)$ of Eq. (6), obtained from the simultaneous fits of $\rho(T)$ and $S(T)$.

A ($\mu\Omega$ cm eV)	δ_1 (meV)	γ_1 (meV)	α	δ_2 (meV)	γ_2 (meV)
392	−43	241	1.13	−9	38

in the stoichiometry and/or by defects in both structure and chemical decoration,[27,28] so that the relative position of the narrow peak can change on this energy scale in samples of slightly different compositions and annealing treatments. Consequently, solely on the basis of small shifts of ε_F, the thermopower of *i*-Al-Cu-Fe samples of similar composition can switch between large positive and large negative values and it may also change sign with temperature, as demonstrated for the $Al_{62}Cu_{25.5}Fe_{12.5}$ and $Al_{63}Cu_{25}Fe_{12}$ polycrystalline samples.[15,16,18] Here, we should also mention that the experimentally observable part of $\rho(\varepsilon)$ in the $\rho(T)$ and $S(T)$ experiments is the one determined by the "thermal observation window" $(-\partial f/\partial\varepsilon)$ [Eqs. (3) and (4)] that is a bell-shaped function centered at the chemical potential μ with a temperature-dependent FWHM $\Delta_f=3.5k_BT$. At $T=300$ K, Δ_f amounts to 90 meV, whereas it becomes as small as 3 meV at 10 K. Upon $T\to 0$, $(-\partial f/\partial\varepsilon)$ becomes a delta function $\delta(\varepsilon-\varepsilon_F)$, and Eq. (3) yields $\rho(T=0)=\rho(\varepsilon_F)$.

The fits of the experimental $\rho(T)$ and $S(T)$ data were performed simultaneously with Eqs. (3)–(6) by adjusting the set of parameters (A, α, δ_1, δ_2, γ_1, and γ_2) pertinent to the shape of the spectral resistivity $\rho(\varepsilon)$. The starting value of the parameter ξ entering the temperature-dependent chemical potential of Eq. (5) was determined by recognizing that in the case when the spectral variation of the electronic diffusivity can be neglected, one can replace $n(\varepsilon)$ by $\sigma(\varepsilon)$ in Eq. (5). ξ can then be related to the thermopower using the Mott formula,

$$S^{Mott}(T) = -\frac{\pi^2}{3}\frac{k_B^2}{|e|}\left[\frac{d\ln\sigma(\varepsilon)}{d\varepsilon}\right]_{\varepsilon_F} T, \tag{7}$$

so that $\xi=-0.5|e|[S^{Mott}(T)/T]$. Taking $S(50\text{ K})=-13.2$ μV/K from Fig. 2(b), we obtain $\xi=0.132$ μeV/K^2 as the initial value. In the fit procedure, ξ was considered as a free parameter, but its final value $\xi=0.145$ μeV/K^2 was close to the initial one. The fits are shown as solid lines in Figs. 2(a) and 2(b) and the fit parameters are collected in Table II. The fits of both $\rho(T)$ and $S(T)$ are excellent in the whole investigated temperature range, except for the small discrepancy at the low-temperature maximum in $\rho(T)$ that cannot be reproduced by this theory (a leveling off towards a T-independent resistivity upon $T\to 0$ is predicted instead).

The spectral resistivity function $\rho(\varepsilon)$ reconstructed from Eq. (6) using the parameter values from Table II is displayed in Fig. 2(c). The narrow Lorentzian has a FWHM $2\gamma_2=76$ meV and its peak is located at $\delta_2=-9$ meV below the Fermi energy, whereas the broad Lorentzian has a width $2\gamma_1=482$ meV and is located $\delta_1=-43$ meV below ε_F. The thermal observation window $-\partial f/\partial\varepsilon$ at $T=300$ K is also shown on the graph. The corresponding spectral conductivity $\sigma(\varepsilon)=1/\rho(\varepsilon)$ is displayed in Fig. 2(d). Fermi energy is located almost at the peak of $\rho(\varepsilon)$, thus in the minimum of the pseudogap in $\sigma(\varepsilon)$. As $\rho(T=0)=\rho(\varepsilon_F)$, this indicates that further shifts of ε_F across the resistivity peak due to deviations in the stoichiometry and/or by defects would not result in additional increase of the resistivity but could just make it smaller. As defects would shift ε_F away from the $\rho(\varepsilon)$ maximum, this also explains why defects decrease the electrical resistivity of less perfect QC samples, thus acting the opposite way as in regular metals. For the given composition and structural quality of the investigated single-crystalline $Al_{64}Cu_{23}Fe_{13}$ sample, ε_F is located practically at the minimum of the pseudogap in $\sigma(\varepsilon)$. Should this be considered as a criterion of the QC perfectness, this sample is a more or less perfect QC (within the limits of the technique), as already indicated by the x-ray and HRTEM structural assessments.

V. THERMAL CONDUCTIVITY

A semiquantitative model of thermal conductivity appropriate to icosahedral QCs and their approximants has been described in the previous investigations of approximant and QC phases in Al-Cr-Fe (Ref. 29) and Al-Pd-Mn (Refs. 30 and 31) systems. The thermal conductivity parameter $\kappa(T)$ is divided into three terms,

$$\kappa(T) = \kappa_{el}(T) + \kappa_D(T) + \kappa_H(T). \tag{8}$$

The electronic contribution κ_{el} is obtained by the Kubo-Greenwood formalism as

$$\kappa_{el}(T) = \frac{L_{22}(T)}{e^2T} - T\sigma(T)S(T)^2, \tag{9}$$

where

$$L_{22}(T) = \int d\varepsilon\sigma(\varepsilon)[\varepsilon-\mu(T)]^2\left[-\frac{\partial f(\varepsilon,T)}{\partial\varepsilon}\right], \tag{10}$$

and $\sigma(T)$ and $S(T)$ are given by Eqs. (3) and (4). In our $\kappa(T)$ analysis, we have calculated κ_{el} by employing the spectral conductivity $\sigma(\varepsilon)$ as determined from the $\sigma(T)$ and $S(T)$ fits (Table II), so that no new fit parameter was introduced.

It is interesting to consider the validity of the empirical Wiedemann-Franz law $\kappa_{el}=L_0T\sigma$ for QCs, where $L_0=\pi^2k_B^2/3e^2$. To this end, Eq. (9) is rewritten by introducing a temperature-dependent effective Lorenz number,

$$L(T) = \frac{\kappa_{el}(T)}{T\sigma(T)}, \tag{11}$$

which should be temperature independent if the empirical Wiedemann-Franz law holds. In the limit $T\to 0$, $L(T)$ goes towards the Wiedemann-Franz value L_0, as can be verified by employing the Sommerfeld expansion of Eq. (11) for low temperatures.[25] For $Al_{64}Cu_{23}Fe_{13}$, the $L(T)$ dependence will be shown in the results section.

The lattice contribution $\kappa_l=\kappa-\kappa_{el}$ is analyzed by considering (i) the propagation of long-wavelength acoustic

phonons (for which the QC structure is an elastic continuum) within the Debye model and (ii) hopping of localized vibrations within the icosahedral cluster substructure, which participate in the heat transfer via thermally activated hopping. In the simplest model, hopping of localized vibrations is described by a single activation energy E_a, yielding a contribution to the thermal conductivity,

$$\kappa_H = \kappa_H^0 \exp(-E_a/k_B T), \tag{12}$$

where κ_H^0 is a constant. The Debye thermal conductivity is written as[32]

$$\kappa_D = C_D T^3 \int_0^{\theta_D/T} \tau(x) \frac{x^4 e^x}{(e^x-1)^2} dx, \tag{13}$$

where $C_D = k_B^4/2\pi^2 \bar{v} \hbar^3$, $\bar{v}$ is the average sound velocity, θ_D the Debye temperature, τ the phonon relaxation time, and $x = \hbar\omega/k_B T$, where $\hbar\omega$ is the phonon energy. The different phonon-scattering processes are incorporated into the relaxation time $\tau(x)$ and we assume that Matthiessen's rule is valid, $\tau^{-1} = \Sigma \tau_j^{-1}$, where τ_j^{-1} is a scattering rate related to the jth scattering channel. In analogy to the Al-Pd-Mn approximant and QC phases,[30,31] we consider two dominant scattering processes in the investigated temperature range (from 2 to 315 K): (1) scattering of phonons on structural defects of stacking-fault-type with the scattering rate $\tau_{sf}^{-1} = Ax^2T^2$ (note that, since $x^2 \propto \omega^2 T^{-2}$, τ_{sf}^{-1} does not show an explicit temperature dependence but frequency dependence, $\tau_{sf}^{-1} \propto \omega^2$) and (2) umklapp processes with the phenomenological form of the scattering rate pertinent to QCs,[29,30,33] $\tau_{um}^{-1} = Bx^\beta T^4$ (yielding frequency and temperature dependence, $\tau_{um}^{-1} \propto \omega^\beta T^{4-\beta}$, where the exponent β should be determined from the fit), so that $\tau^{-1} = \tau_{sf}^{-1} + \tau_{um}^{-1}$.

The Debye temperature of *i*-Al-Cu-Fe was estimated from specific heat[34] as $\theta_D \approx 560$ K. Since our $\kappa(T)$ data are available only up to 315 K, it turned out that the fit was insensitive to a slight change of this θ_D value, so that a fixed $\theta_D = 500$ K was used. The Debye constant C_D was also not taken as a free parameter but was instead calculated using $\bar{v} = 4000$ ms^{-1}, a quite common value for Al-based icosahedral QCs, as determined from ultrasonic data.[35]

The thermal conductivity of $Al_{64}Cu_{23}Fe_{13}$ was measured along the threefold symmetry direction using an absolute steady-state heat flow method. The thermal flux was generated by a 1 kΩ RuO_2 chip resistor, glued to one end of the sample, while the other end was attached to a copper heat sink. The temperature gradient across the sample was monitored by a chromel-constantan differential thermocouple. The temperature-dependent thermal conductivity $\kappa(T)$ is displayed in Fig. 3(a). The conductivity value is low in the whole investigated temperature interval from 2 to 315 K, amounting at RT to $\kappa_{300\ \mathrm{K}} = 1.7$ W/m K. This value is surprisingly low for an alloy of regular metals and is even lower than the thermal conductivities of known thermal (and electrical) insulators amorphous[36] SiO_2 with $\kappa_{300\ \mathrm{K}} = 2.8$ W/m K and the technologically widespread thermally insulating material yttrium-doped zirconia ceramics[37] $Zr_{1-x}Y_xO_{2-x/2}$ ($x < 0.2$), where $\kappa_{300\ \mathrm{K}} = 2$ W/m K.

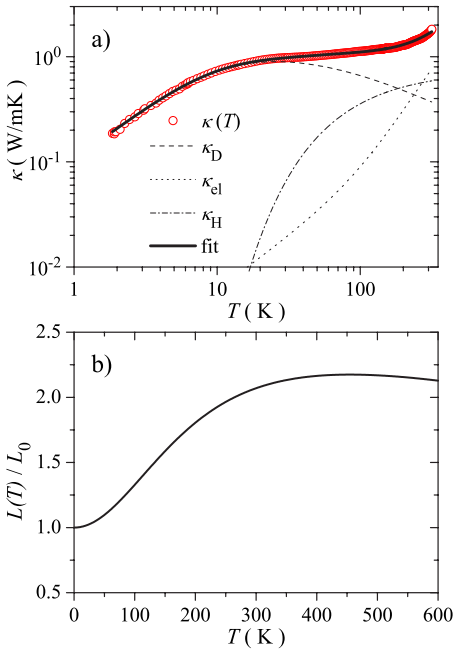

FIG. 3. (Color online) (a) Temperature-dependent thermal conductivity $\kappa(T)$ of the single-crystalline $Al_{64}Cu_{23}Fe_{13}$. The fit (solid line) was made by Eq. (8) and the three contributions to the total $\kappa(T)$ (electronic κ_{el}, Debye κ_D, and hopping κ_H) are shown separately. (b) Temperature-dependent effective Lorenz number calculated from Eq. (11).

The $\kappa(T)$ data were analyzed by means of Eq. (8). The fit [solid line in Fig. 3(a)] is excellent and the fit parameters are collected in Table III. The electronic (κ_{el}), Debye (κ_D), and hopping (κ_H) contributions are shown separately on the graph. The temperature-dependent effective Lorenz number $L(T)$ of Eq. (11) is displayed in Fig. 3(b). At temperatures away from the $T \to 0$ regime, $L(T)$ deviates considerably from the Wiedemann-Franz value L_0, amounting to $L/L_0 = 2.1$ at 300 K. The RT value of the electronic contribution amounts to $\kappa_{el}^{300\ \mathrm{K}} = 0.69$ W/m K, so that at RT, the electrons carry 40% of the total heat. The Debye contribution exhibits a maximum at about 30 K and declines above, whereas the hopping contribution becomes significant at elevated temperatures. The activation energy for hopping was determined as $E_a \approx 6$ meV, which correlates with the inelastic neutron[38–40] and x-ray[41] scattering experiments on *i*-Al-Pd-Mn QCs, where dispersionless vibrational states were identified for energies higher than 12 meV. Such dispersionless states indicate localized vibrations and are considered to be a consequence of a dense distribution of energy gaps in the phonon excitation spectrum of QCs. The parameters B and β define phonon scattering by umklapp processes

TABLE III. Fit parameters of the thermal conductivity $\kappa(T)$ from Fig. 3(a).

κ_H^0 (W/m K)	E_a (meV)	A (s^{-1} K^{-2})	B (s^{-1} K^{-4})	β
0.7±0.1	6.3±0.3	1.2×10^7	2.8×10^4	3.2±0.2

in a phenomenological way. The fit-determined $\beta=3.2$ value yields the frequency and temperature dependence of the umklapp term $\tau_{um}^{-1} \propto \omega^{3.2} T^{0.8}$, indicating similarity to the modified quasiumklapp scattering rate $\tau_{um}^{-1} \propto \omega^3 T$, used for the analysis of thermal conductivity of *i*-Zn-Mg-Y QC.[42] Here, it should be mentioned that the Debye and hopping contributions slightly compensate each other in the fit procedure, so that the parameter values characterizing κ_D and κ_H should be considered at the qualitative level.

VI. DISCUSSION

We now make comparison of the above-presented physical properties of the $Al_{64}Cu_{23}Fe_{13}$ single-crystalline QC to literature reports on the polycrystalline *i*-Al-Cu-Fe material. Considering the magnetic properties, magnetic susceptibility of the $Al_{64}Cu_{23}Fe_{13}$ is negative in most of the investigated temperature interval (except below 7 K), but the residual magnetic Fe fraction $f \approx 2 \times 10^{-4}$ is still substantial, so that the sample should be best classified as a weak Curie paramagnet rather than a diamagnet. As a practically identical magnetic Fe fraction was reported also for the polycrystalline $Al_{63}Cu_{25}Fe_{12}$ QC,[14] there appears to be no significant difference in the magnetic properties of the single-crystalline and polycrystalline *i*-Al-Cu-Fe materials. A similar result of a diamagnetic susceptibility with a Curie upturn observable at temperatures below 30 K was reported for another polycrystalline $Al_{63}Cu_{25}Fe_{12}$ sample,[9] where the paramagnetic magnetization of the as-quenched sample was reduced upon annealing (in Ref. 9, the figures of the magnetic Fe fractions are not given). It was proposed that this paramagnetism could be due to parasitic crystalline phases or structural defects, thus of extrinsic origin to the *i*-Al-Cu-Fe phase. Our results on high-quality $Al_{64}Cu_{23}Fe_{13}$ suggest that the observed marginal magnetism is an intrinsic property of the *i*-Al-Cu-Fe phase and the small magnetic Fe fraction is an equilibrium phenomenon. In a theoretical work on Al-TM QCs (TM stands for transition metal),[43,44] it was shown that the magnetism can be discussed in terms of a local electronic DOS at the TM sites. The appearance of a magnetic moment at a particular TM site (e.g., Fe in *i*-Al-Cu-Fe or Mn in *i*-Al-Pd-Mn) within the QC structure depends on the local DOS at that site, which is sensitive to the nearby local atomic environment up to 5–10 Å. Surrounding of TM atoms by predominantly Al atoms results in strong *sp-d* hybridization, which favors a nonmagnetic state, whereas surrounding by more TM and less Al reduces the *sp-d* hybridization and TM consequently becomes magnetic. Extended x-ray-absorption fine structure study[45] of the local Fe environments in polycrystalline $Al_{63}Cu_{25}Fe_{12}$ QC has revealed that the nearest-neighbor coordination shell of the Fe atoms contains Al atoms only without direct contacts to other Fe, accounting for the nonmagnetic character of most of the Fe sites. According to the local DOS criterion, there are many TM sites in the *i*-Al-Cu-Fe structure that are close to a magnetic-nonmagnetic transition, so that a small fraction of these are magnetic and the observed marginal magnetism is of intrinsic origin to the *i*-Al-Cu-Fe phase. This picture can also explain the reduction of magnetization upon annealing in the Al-TM QCs, which is due to a redistribution of atomic species and vacancies around the TM atoms via thermal diffusion in a way to create preferentially more Al-rich environments. Upon annealing, the magnetic moments at some TM sites in the as-grown material consequently disappear.

It is also worth commenting on the appropriateness of the term "small magnetic fraction" in the analysis of the *i*-Al-Cu-Fe (or generally *i*-Al-TM QCs) magnetism, as frequently used in literature. What we measure experimentally is the total paramagnetic magnetization of all the Fe atoms. Assuming a particular ionization state of the Fe atom (e.g., Fe^{2+}), further analysis is made due to simplicity reasons in the "all-or-nothing" manner, by considering that an Fe atom is either nonmagnetic or it possesses the full Fe^{2+} magnetic moment. Since the paramagnetic magnetization is small, such an analysis then yields a small number of magnetic Fe sites. In view of the fact that many Fe sites in the *i*-Al-Cu-Fe structure are close to a magnetic-nonmagnetic transition, many Fe sites may alternatively carry reduced magnetic moments (due to partial spin compensation by the conduction-electron cloud), so that the magnetic Fe fraction may in reality not be small. What is small is their total paramagnetic magnetization.

The magnitude of the electrical resistivity and $\rho(T)$ of the single-crystalline $Al_{64}Cu_{23}Fe_{13}$ ($\rho_{300\ K}=2200\ \mu\Omega$ cm, $\rho_{4\ K}=3950\ \mu\Omega$ cm, and $R=1.8$) are in-line with the values reported for the polycrystalline *i*-Al-Cu-Fe. Similar values ($\rho_{300\ K}=2630\ \mu\Omega$ cm, $\rho_{4\ K}=4800\ \mu\Omega$ cm, and $R=1.82$) were reported for polycrystalline[14] $Al_{63}Cu_{25}Fe_{12}$, whereas $3600\ \mu\Omega\ \text{cm} < \rho_{4\ K} < 10\,000\ \mu\Omega$ cm values were reported for several polycrystalline samples of slightly varying icosahedral composition ($12\% < \text{Fe} < 13\%$).[7,9–13,15] The crucial role of Fe in determining the magnitude of the electrical resistivity of *i*-Al-Cu-Fe QCs has been elaborated in a study[11] that involved a large number 20 of rapidly quenched ribbons with a different Fe content over the icosahedral concentration range $12\% < \text{Fe} < 13\%$. The results revealed that the resistivity best correlates with the Fe content rather than with the electron-per-atom ratio e/a, showing the importance of *d* states in the resistivity of *i*-Al-Cu-Fe. Being a function of the Fe content, $\rho_{4\ K}$ exhibited a maximum for the 12.5% Fe concentration where it amounted to $\rho_{4\ K} \approx 8000\ \mu\Omega$ cm, whereas at both edge Fe concentrations (12% and 13%), it amounted to $\rho_{4\ K} \approx 4000\ \mu\Omega$ cm. This high-resolution Fe-concentration study elucidates the question on the possible resonance effect in the resistivity versus Fe composition that could yield to a very high resistivity at a particular sharp Fe concentration and a proximity of a metal-to-insulator transition.[9] In polycrystalline *i*-Al-Cu-Fe, the total variation of ρ over the relevant Fe range is merely a factor of 2,[11] so that the material is best classified as a semimetal over the whole icosahedral concentration range with no indication of a large resonant increase of the resistivity. The $\rho_{4\ K}$ resistivity value of our single-crystalline $Al_{64}Cu_{23}Fe_{13}$ matches well that of the polycrystalline samples from the study[11] with the same Fe concentration. However, since the Fermi energy of our $Al_{64}Cu_{23}Fe_{13}$ is located nearly at the maximum of the spectral resistivity [Fig. 2(c)], further shifts of ε_F over the resistivity peak due to small variation of the Fe composition

would not result in an additional increase of the resistivity but can only make it smaller. This hints that the factor of 2 larger peak resistivity of the polycrystalline *i*-Al-Cu-Fe material at the 12.5% Fe concentration,[11] as compared to the single-crystalline $Al_{64}Cu_{23}Fe_{13}$, could originate from extrinsic factors such as grain boundaries and other lattice imperfections that act as additional scattering centers for the conduction electrons.

It is instructive to consider other theoretical approaches reported so far in literature for reproducing temperature-dependent electron-transport parameters of *i*-Al-Cu-Fe. While there were many successful attempts to explain single quantities (e.g., the electrical resistivity alone), simultaneous fits of more than one quantity by the same theoretical model (and fit parameter values) are scarce. In Ref. 13, the electrical resistivity $\Delta\rho(T)$ and magnetoresistance $\Delta\rho(B,T)$ of polycrystalline *i*-Al-Cu-Fe were analyzed by considering quantum interference effects (weak localization theory and electron-electron interactions). Simultaneous fits of both quantities were successfully made in the low-temperature regime up to 150 K, though the magnetoresistance alone could be fitted up to 280 K. A quite different approach was employed in Refs. 15 and 16, where the resistivity, thermopower, and Hall coefficient R_H of polycrystalline $Al_{62}Cu_{25.5}Fe_{12.5}$ and $Al_{63}Cu_{25}Fe_{12}$ were analyzed simultaneously by using a two-band model of electrons and holes that are thermally excited into conduction across the semiconducting gap of width $E_G \approx 30$ meV. Considering temperature-dependent electron and hole densities (showing nonzero densities at $T=0$), their effective masses and scattering times as free parameters, $\rho(T)$, $S(T)$, and $R_H(T)$, were successfully reproduced simultaneously in the whole investigated temperature range, 4–340 K.

Regarding comparison of the thermal conductivity of single-crystalline and polycrystalline *i*-Al-Cu-Fe, we are not aware of other quantitative analyses of $\kappa(T)$ of polycrystalline samples in the sense of Eqs. (8)–(13), so that comparison has to be made at the level of experimental thermal conductivities. The RT value for the single-crystalline $Al_{64}Cu_{23}Fe_{13}$ amounts to $\kappa_{300\ K}=1.7$ W/m K, whereas the reported figures for the polycrystalline samples are $\kappa_{300\ K}=6$ W/m K for $Al_{62}Cu_{25.5}Fe_{12.5}$ and $\kappa_{300\ K}=2.9$ W/m K for $Al_{63}Cu_{25}Fe_{12}$ (Ref. 15) and $\kappa_{220\ K}=0.9$ W/m K for $Al_{62.5}Cu_{25}Fe_{12.5}$ (Ref. 18, where the highest reported temperature is 220 K). Though the scatter of these values is relatively large, there seems to be no systematic difference between the polycrystalline and single-crystalline samples.

VII. CONCLUSIONS

In order to test for the true intrinsic properties of *i*-Al-Cu-Fe QCs, we performed investigations of magnetism, electrical resistivity, thermoelectric power, and thermal conductivity on a single-crystalline $Al_{64}Cu_{23}Fe_{13}$ QC, grown directly from the melt by the Czochralski technique. Based on x-ray and HRTEM structural evaluations,[21] this sample shows superior quasicrystallinity and an almost phason-free structure. Its superior thermal stability[2] suggests that the sample could be at the ideal icosahedral composition. Our electrical resistivity and thermopower analysis shows that the Fermi energy is located at the minimum of the pseudogap in the spectral conductivity $\sigma(\varepsilon)$. All these give evidence that we are dealing with an icosahedral QC sample of exceptional quality, so that its physical properties may be considered as intrinsic to the *i*-Al-Cu-Fe phase. In contrast, one can suspect that phason strain, a too high vacancy concentration for the RT conditions, and grain boundaries in the rapidly solidified polycrystalline material may influence the measured physical properties to the extent that the true intrinsic properties of the *i*-Al-Cu-Fe phase are obscured by a finite quality of the polycrystalline material.

A comparison of the investigated single-crystalline $Al_{64}Cu_{23}Fe_{13}$ to the literature reports on polycrystalline *i*-Al-Cu-Fe, however, shows that there are no pronounced differences between the two forms of the material. While there are essentially no differences in the magnetic properties of the single-crystalline and polycrystalline materials, the electrical resistivity of the polycrystalline material is larger by a factor of 2. This difference can be easily brought in by the grain boundaries and other lattice imperfections that act as additional scattering centers for the conducting electrons. Comparing thermopowers of the single-crystalline and polycrystalline *i*-Al-Cu-Fe materials, the $S(T)$ magnitude and temperature dependence depends strongly on the position of ε_F relative to the spectral resistivity peak, so that slight differences in the samples' stoichiometry and structural perfection may lead to very different thermopowers in both magnitude and sign. The available $S(T)$ data suggest that the thermopower of the single-crystalline $Al_{64}Cu_{23}Fe_{13}$ is not significantly different from those reported for the polycrystalline *i*-Al-Cu-Fe samples [e.g., $S(T)$ of polycrystalline[11] $Al_{63}Cu_{25}Fe_{12}$ is very similar in magnitude and T dependence to our $Al_{64}Cu_{23}Fe_{13}$]. Quantitative comparison of the thermal conductivities of single-crystalline and polycrystalline *i*-Al-Cu-Fe is less straightforward due to random scatter of the reported values, but $\kappa_{300\ K}$ of the single-crystalline $Al_{64}Cu_{23}Fe_{13}$ fits within the range of values reported for the polycrystalline samples.

To conclude, we found no systematic differences in the magnetism, electrical resistivity, thermoelectric power, and thermal conductivity between the high-quality single-crystalline and polycrystalline *i*-Al-Cu-Fe QCs, except for the trivial hindering of long-range transport by grain boundaries in the polycrystalline material. In this sense, the so far reported physical properties of *i*-Al-Cu-Fe QCs appear to be intrinsic to this family of icosahedral QCs, regardless of the form of the material.

ACKNOWLEDGMENT

A.S. acknowledges support by the Ministry of Science, Education and Sports of the Republic of Croatia through Research Project No. 177-0352828-0478, "Transport and magnetic properties of nanostructured complex metallic compounds."

[1] A. P. Tsai, A. Inoue, and T. Masumoto, Jpn. J. Appl. Phys., Part 2 **26**, L1505 (1987).
[2] Y. Yokoyama, R. Note, K. Fukaura, H. Sunada, K. Hiraga, and A. Inoue, Mater. Trans., JIM **41**, 1583 (2000).
[3] Y. Yokoyama, K. Fukaura, and H. Sunada, Mater. Trans., JIM **41**, 668 (2000).
[4] A. Smontara, J. C. Lasjaunias, C. Paulsen, A. Bilušić, and Y. Calvayrac, Mater. Sci. Eng., A **294-296**, 706 (2000).
[5] T. Ishimasa and M. Mori, Philos. Mag. Lett. **62**, 357 (1990).
[6] T. A. Lograsso and D. W. Delaney, J. Mater. Res. **11**, 2125 (1996).
[7] T. Klein, A. Gozlan, C. Berger, F. Cyrot-Lackmann, Y. Calvayrac, and A. Quivy, Europhys. Lett. **13**, 129 (1990).
[8] T. A. Lograsso and D. W. Delaney, *Proceedings of the 6th International Conference on Quasicrystals*, edited by S. Takeuchi and T. Fujiwara (World Scientific, Singapore, 1997), p. 325.
[9] T. Klein, C. Berger, D. Mayou, and F. Cyrot-Lackmann, Phys. Rev. Lett. **66**, 2907 (1991).
[10] T. Klein, H. Rakoto, C. Berger, G. Fourcaudot, and F. Cyrot-Lackmann, Phys. Rev. B **45**, 2046 (1992).
[11] P. Lindqvist, C. Berger, T. Klein, P. Lanco, F. Cyrot-Lackmann, and Y. Calvayrac, Phys. Rev. B **48**, 630 (1993).
[12] D. Mayou, C. Berger, F. Cyrot-Lackmann, T. Klein, and P. Lanco, Phys. Rev. Lett. **70**, 3915 (1993).
[13] M. Ahlgren, P. Lindqvist, M. Rodmar, and Ö. Rapp, Phys. Rev. B **55**, 14847 (1997).
[14] R. Escudero, J. C. Lasjaunias, Y. Calvayrac, and M. Boudard, J. Phys.: Condens. Matter **11**, 383 (1999).
[15] A. Bilušić, A. Smontara, J. C. Lasjaunias, J. Ivkov, and Y. Calvayrac, Mater. Sci. Eng., A **294-296**, 711 (2000).
[16] A. Bilušić, I. Bešlić, J. Ivkov, J. C. Lasjaunias, and A. Smontara, Fiz. A **8**, 183 (1999).
[17] C. V. Landauro and H. Solbrig, Mater. Sci. Eng., A **294-296**, 600 (2000).
[18] H. Solbrig and C. V. Landauro, in *Quasicrystals, Structure and Physical Properties*, edited by H.-R. Trebin (Wiley-VCH, Weinheim, 2003), p. 254.
[19] A. Perrot, J. M. Dubois, M. Cassart, and J. P. Issi, *Proceedings of the 5th International Conference on Quasicrystals*, edited by C. Janot and R. Mosseri (World Scientific, Singapore, 1995), p. 588.
[20] See, for a review, K. Fukamichi, in *Physical Properties of Quasicrystals*, edited by Z. M. Stadnik (Springer, New York, 1999), p. 295, and references therein.
[21] Y. Yokoyama, Y. Matsuo, K. Yamamoto, and K. Hiraga, Mater. Trans., JIM **43**, 762 (2002).
[22] P. W. Selwood, *Magnetochemistry* (Interscience, New York, 1956), p. 78.
[23] A. Kobayashi, S. Matsuo, T. Ishimasa, and H. Nakano, J. Phys.: Condens. Matter **9**, 3205 (1997).
[24] F. E. Mabbs and D. J. Machin, *Magnetism and Transition Metal Complexes* (Chapman and Hall, London, 1973), p. 7.
[25] C. V. Landauro and H. Solbrig, Physica B **301**, 267 (2001); C. V. Landauro, Ph.D. thesis, TU Chemnitz, 2002 (http//archive.tu-chemnitz.de/pub/2002/).
[26] N. W. Aschroft and N. D. Mermin, *Solid State Physics* (Saunders College Publishing, London, 1976), p. 46.
[27] F. S. Pierce, P. A. Bancel, B. D. Biggs, Q. Guo, and S. J. Poon, Phys. Rev. B **47**, 5670 (1993).
[28] H. Solbrig, C. V. Landauro, and A. Löser, Mater. Sci. Eng., A **294-296**, 596 (2000).
[29] Ž. Bihar *et al.*, J. Alloys Compd. **407**, 65 (2006).
[30] J. Dolinšek, P. Jeglic, P. J. McGuiness, Z. Jaglicic, A. Bilusic, Z. Bihar, A. Smontara, C. V. Landauro, M. Feuerbacher, B. Grushko, and K. Urban, Phys. Rev. B **72**, 064208 (2005).
[31] A. Bilušić, A. Smontara, J. Dolinšek, P. J. McGuiness, and H. R. Ott, J. Alloys Compd. **432**, 1 (2007).
[32] R. Bergman, *Thermal Conduction in Solids* (Oxford University Press, New York, 1978).
[33] P. A. Kalugin, M. A. Chernikov, A. Bianchi, and H. R. Ott, Phys. Rev. B **53**, 14145 (1996).
[34] J. C. Lasjaunias, Y. Calvayrac, and H. Yang, J. Phys. I **7**, 959 (1997).
[35] Y. Amazit, M. de Boissieu, and A. Zarembowitch, Europhys. Lett. **20**, 703 (1992).
[36] D.-M. Zhu, Phys. Rev. B **50**, 6053 (1994).
[37] R. Mévrel, J.-C. Laizet, A. Azzopardi, B. Leclercq, M. Poulain, O. Lavigne, and D. Demange, J. Eur. Ceram. Soc. **24**, 3081 (2004).
[38] C. Janot, A. Magerl, B. Frick, and M. de Boissieu, Phys. Rev. Lett. **71**, 871 (1993).
[39] M. de Boissieu, M. Boudard, R. Bellisent, M. Quilichini, B. Hennion, R. Currat, A. I. Goldman, and C. Janot, J. Phys.: Condens. Matter **5**, 4945 (1993).
[40] M. Boudard, M. de Boissieu, S. Kycia, A. I. Goldman, B. Hennion, R. Bellisent, M. Quilichini, R. Currat, and C. Janot, J. Phys.: Condens. Matter **7**, 7299 (1995).
[41] M. Krisch, R. A. Brand, M. A. Chernikov, and H. R. Ott, Phys. Rev. B **65**, 134201 (2002).
[42] K. Giannó, A. V. Sologubenko, M. A. Chernikov, H. R. Ott, I. R. Fisher, and P. C. Canfield, Phys. Rev. B **62**, 292 (2000).
[43] G. Trambly de Laissardière and D. Mayou, Phys. Rev. Lett. **85**, 3273 (2000).
[44] G. Trambly de Laissardière and D. Mayou, Mater. Sci. Eng., A **294-296**, 621 (2000).
[45] J. Padežnik Gomilšek, I. Arčon, A. Kodre, and J. Dolinšek, Solid State Commun. **123**, 527 (2002).